

A&A manuscript no.
(will be inserted by hand later)

Your thesaurus codes are:
11 (11.14.1; 11.17.3; 11.17.4; 11.10.1)

**ASTRONOMY
AND
ASTROPHYSICS**

Gamma-ray to radio activity and ejection of a VLBI component in the jet of the S5-quasar 0836+710

K. Otterbein^{1,3}, T. P. Krichbaum¹, A. Kraus¹, A. P. Lobanov¹, A. Witzel¹, S. J. Wagner², and J. A. Zensus¹

¹ Max-Planck-Institut für Radioastronomie, Auf dem Hügel 69, D-53121 Bonn, Germany

² Landessternwarte Heidelberg, Königstuhl, D-69117 Heidelberg, Germany

³ Now at: Landessternwarte Heidelberg, Königstuhl, D-69117 Heidelberg, Germany

Received ; accepted

Abstract. Broad-band (gamma to radio) variations of the flux density were observed in the first half of 1992 in the luminous high redshift ($z = 2.172$) quasar S5 0836+710. VLBI monitoring observations during 1993 – 1996 performed at 86 GHz, 22 GHz, 15 GHz, and 8 GHz show the ejection of a new jet component, which most probably is directly related to a quasi simultaneous gamma-, X-ray, optical flaring activity which was observed in February 1992. During the period 1992 – 1993 the flaring propagated through the radio spectrum. From several quasi-simultaneous radio spectra taken during this phase of activity, we determine the time evolution of the spectral turnover of the radio spectrum in the $S_m - \nu_m$ diagram. The data indicate a correlation of the jet activity with the variability of the broad-band electromagnetic spectrum of the source. The observational findings are discussed in the framework of relativistic shock models.

Key words: galaxies: nuclei – quasars: general – quasars: S5 0836+710 – galaxies: jets

1. Introduction

In early 1992, the ultraluminous S5 quasar 0836+710 (4C 71.07, $z = 2.172$) underwent a prominent optical outburst (von Linde et al. 1993), which later led to enhanced variability in the mm- and cm- radio bands (Marscher and Bloom 1994). At the time of the optical flaring, the source also was in a bright state in the gamma-regime (EGRET: Fichtel et al. 1994) and at soft X-rays (ROSAT: Brunner et al. 1994). Motivated by the increased activity of the source, we started a high frequency VLBI monitoring program in 1993 in order to investigate the possible relation between broad-band changes in the flux density and structural variations in the jet on sub-milliarcssecond scales. The ejection of new VLBI jet components after major outbursts in the flux density has been observed also in a few other sources (e. g. component ejection after optical flaring: 3C 345

Babadzhanyants and Belokon 1986, 3C 273 Krichbaum et al. 1990a; ejection after radio flares: BL Lac Mutel et al. 1990, PKS 0420–014, Wagner et al. 1995a) and seems to be a quite common phenomenon in compact flat spectrum radio sources (blazars).

With the new data obtained for 0836+710, it appears very likely that the relation between outbursts in the flux density observed at high frequencies and jet component ejection is not limited to the synchrotron regime (e.g. optical-to-radio), but most probably covers a much wider spectral range (gamma-to-radio), possibly the full electromagnetic spectrum. Similar correlations between gamma-activity and jet activity were recently found also in a number of other sources, e.g. in 3C 273 (Krichbaum et al. 1996), 3C 279 (Wehrle et al. 1994), 0528+134 and 3C454.3 (Krichbaum et al. 1995), where the ejection of jet components could be related to gamma-flares, or enhanced levels of gamma-activity. However, in most of the published cases the frequency coverage is not as broad as presented here for 0836+710.

The quasar 0836+710 is a member of a complete flux density limited sample of 13 flat-spectrum radio sources (Eckart et al. 1986 & 1987) compiled from the 6 cm S5 survey (Kühr et al. 1981). The 13 sources of the sample are located in the northern polar cap ($\delta \geq 70^\circ$) and are regularly studied with VLBI at frequencies ranging from 0.3 to 22 GHz (cf. Witzel et al. 1988 and references therein). The VLBI data for 0836+710 now span a time range of more than 15 years (1983–1996).

The high dynamic range VLBI images of 0836+710 reveal a complex and wiggled one-sided core-jet structure (Eckart et al. 1986, Eckart et al. 1987). World-array VLBI images at 90 cm and 18 cm show the jet extending over more than 150 milliarcseconds (mas) in direction to the outer arcsecond lobe seen with MERLIN and the VLA (Hummel et al. 1992). Mainly from the VLBI monitoring at 6 cm (Krichbaum et al. 1990b hereafter K90b, Otterbein 1996 hereafter O96), a very complex motion pattern is revealed, with jet components, moving at velocities ranging from subluminal ($\beta_{app} = 0.5$; $\beta = v/c$) to superluminal ($\beta_{app} = 10$) (assuming $H_0 = 100 \text{ km/s/Mpc}$ and $q_0 = 0.5$, throughout this paper). No systematic correlation between the speed of the jet and the separation of the components from the core seems to be present. The jet shows a noticeably

Table 1. Summary of experiments

date	freq. [GHz]	observing mode, bandwidth [MHz]	array
1993, Apr. 7	86.2	MK III (A), 112	global (4) ¹
1993, Sep. 16	22.2	MK III (B), 56	global (11)
1995, Jan. 20	15.3	VLBA 64-8-1, 32	VLBA (10) ²
1995, Aug. 24	22.2	VLBA 128-8-1,64	VLBA (10) ³
1995, Aug. 24	8.4	VLBA 128-8-1,64	VLBA (10) ³

Notes:

¹: stations: Effelsberg, Pico Veleta, Onsala, Haystack

²: snapshot-type observations

³: 8/22 GHz simultaneous dual-frequency observations

structure, with lateral displacements of its ridge line (kinks) and oscillations of its transverse width (K90b).

At cm-wavelengths, 0836+710 is strongly polarized ($p \simeq 9\%$ at 5 GHz). Polarization VLBI images show a highly polarized jet with the magnetic field roughly following the bent ridge line (Cawthorne et al. 1993). This suggests that the jet of 0836+710 is also highly magnetized.

In this paper, we focus on the structural changes observed in the sub-milliarcsecond regions of the inner jet of 0836+710 during and after the optical outburst of 1992. A more detailed discussion of the overall morphology and the spectral and kinematic properties of the milliarcsecond-jet will be given elsewhere.

2. Observations and data reduction

0836+710 was observed with VLBI between 1993 and 1995 at frequencies ranging from 8 GHz to 86 GHz. The observations in August 1995 were made in dual-frequency mode (22 and 8 GHz). At 86 GHz and 15 GHz¹ the data for 0836+710 were obtained during VLBI campaigns which also included other sources (86 GHz: Schalinski et al. 1994; 15 GHz: Patnaik et al. 1996). Owing to the limited *uv*-coverage in the 86 and 15 GHz data sets, the dynamic range of the corresponding maps is lower than that of the high dynamic range images at 22 and 8 GHz, with their optimal *uv*-coverage. The details of the observations are summarized in Table 1. Column 1 gives the observing date, column 2 the frequency, column 3 the observing mode and bandwidth, and column 4 the VLBI array with the number of participating stations in brackets.

After the correlation (VLBA data in Socorro, MK III data in Bonn), the data were fringe-fitted and calibrated in the standard manner. AIPS was used for reducing the VLBA data. The fringe fitting of the MK III data was done using the Haystack software (Rogers et al. 1983), and the baseline oriented global fringe fitting routines available at the MPIfR (Alef & Porcas 1986, Alef 1989). The amplitude calibration was carried out in the standard way, using system temperature measurements and elevation-dependent antenna gain curves. At 22 GHz and

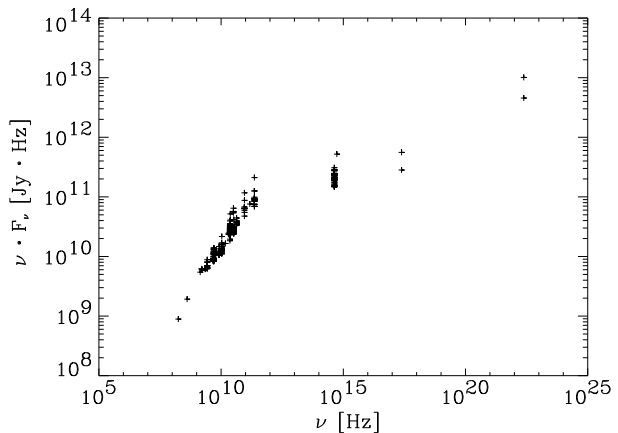


Fig. 1. Overall spectrum (νF_ν) of 0836+710 as compiled from presented and published data.

86 GHz we included corrections for atmospheric absorption (opacity) in the amplitude calibration.

The imaging was performed using the CalTech VLBI package and the difference mapping software DIFMAP (Pearson 1991, Shepherd et al. 1994). In parallel to the mapping, we made Gaussian model fits to the visibility amplitudes and phases, in order to parameterize the multi-component structures seen in the maps. The measurement errors of the parameters of the Gaussian components were determined formally from least square fits and, in addition, from their variations on fits to slightly different calibrated and edited data sets.

3. Results

3.1. Broad-band Variability

0836+710, which in the past showed only mild variations of its radio flux density, recently changed into a more active phase of variability. Between 1990–1993 the source exhibited strong variability, which seems to be correlated over a wide range of the electromagnetic spectrum. In Figure 1, we show the total luminosity spectrum; and in Figure 2, we show the flux density measurements for the interval 1990.5–1993.2. The data are taken from the literature and include, from the top to the bottom, EGRET observations in the gamma-band at 100 MeV (Mukherjee et al. 1997), ROSAT observations in the X-ray band at 1 keV (Brunner et al. 1994), optical R-band observations (von Linde et al. 1993, Schramm et al. 1994 and Heidelberg telescope), 230 GHz and 90 GHz flux density measurements from the IRAM 30 m millimeter telescope at Pico Veleta and from the JCMT at Mauna Kea (Steppe et al. 1993, Bloom et al. 1994), and measurements at 43, 37 and 22 GHz from the Metsähovi flux density monitoring program (E. Valtaoja, priv. comm.) and from the 100 m radio telescope at Effelsberg.

From Figure 2, it is clear that the sparse and irregular time sampling, particularly in the X-ray and gamma-bands, requires

¹ The 15 GHz data were kindly provided by A. Patnaik

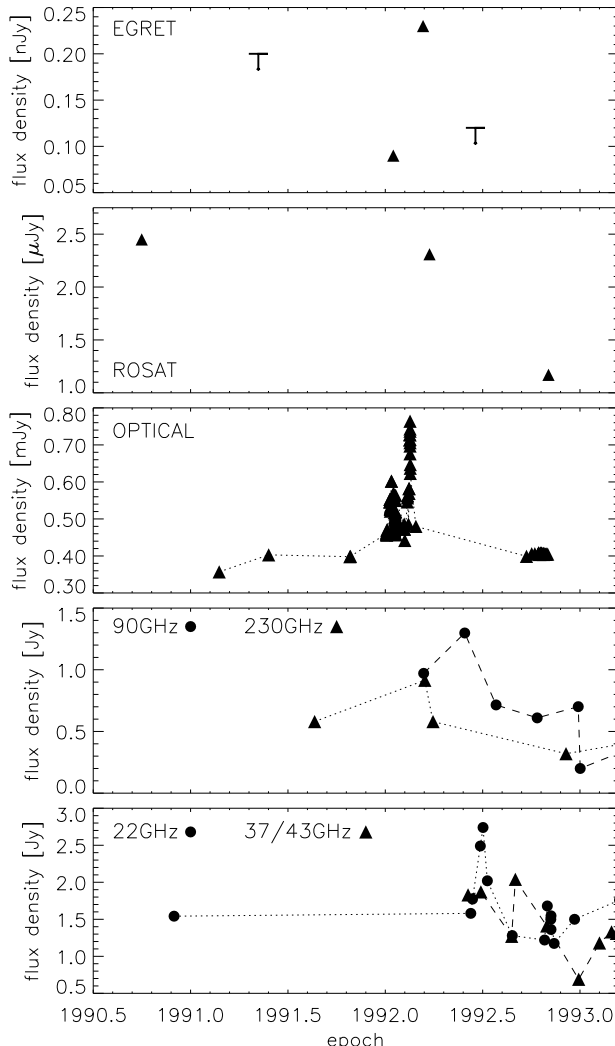


Fig. 2. Broad-band flux density variability in 0836+710 for the period 1990.5 – 1993.2. From top to bottom gamma-ray, X-ray, optical, millimeter- and cm-radio data are shown (for origin of data see text). The lines connect adjacent data points, arrows in the top panel indicate upper limits. The data suggest a correlated gamma- to optical outburst first peaking in 1992.13, and propagating later towards longer (mm-/cm-) wavelengths.

a careful interpretation. Obviously, a cross correlation analysis, or an accurate determination of the time lags between the different bands is not possible. The data nevertheless indicate a tight correlation between the gamma-/X-ray and optical flux density levels. Close to the optical flaring activity observed in 1992.1–1992.2, the gamma- and X-ray flux density was also high. The EGRET measurements show variability by a factor of 2–3 on a time scale of < 0.5 yrs, and low flux densities shortly before and after the time of the optical flaring. The X-ray flux is also variable. About 0.5 years after the optical outburst, it dropped by a factor of 2. Given the sparse sampling, the data are consistent with a (at least nearly) simultaneous ($\Delta t \leq 0.1$ yrs) gamma-ray/optical flaring. This is

consistent with nearly simultaneous gamma-/optical variations observed in a few other objects, eg. in 1406–076 (Wagner et al. 1995b). From the measurements in the mm- and cm-bands it appears that the optical outburst propagates towards longer wavelengths, with the maximum in the radio appearing after $0.1 – 0.3$ yrs first at shorter (mm-), and after $0.3 – 0.5$ yrs later at longer (cm-) wavelengths.

3.2. Results from the VLBI monitoring

3.2.1. Overall morphology and component identification

In Figure 3, we show two 22 GHz images of 0836+710 obtained in 1993.71 and 1995.65. As in the maps obtained earlier at longer wavelengths, the source shows a one sided core/jet structure with several compact components. From the maps and the model fits, we identified several distinct jet components B3, B2, B, and C1 (B and C1 are blended) located at separations from the core of up to $r \simeq 4$ mas. The labels in Figure 3 reflect this identification scheme, in which we implicitly assumed that the brightest component located at the map center is the stationary core of the jet. Beyond a separation of 4 mas from the core, the jet emission becomes weaker and more extended, so that it is resolved by the interferometer beam. Images obtained by applying a taper to the 22 GHz *uv*-data, however, show that the emission from the jet extends to 15 mas from the core, in good agreement with the outer structure seen previously at longer wavelengths (K90b, Hummel et al. 1992).

In the following, we use a component annotation similar to the one introduced by K90b for the 5 GHz data. The feature seen at a separation of $r \sim 3$ mas from the core can be identified as a blend between a fast moving older 5 GHz component B ($\beta_{app} = 9.6 \pm 0.2$; $\beta = v/c$) and a quasi-stationary component C1 ($\beta_{app} \leq 2$). Near component C1, the jet direction changes. This displacement is seen more clearly in the 'tapered' 22 GHz images, and also in the maps at 15 and 8 GHz. We note that similar displacements also appear at larger separations from the core, in particular near component D at $r \simeq 10$ mas in the 5 GHz maps (K90b), and near component G2 at $r \simeq 30$ mas (Hummel et al. 1992) at 1.6 GHz. With the new 22 GHz maps, it appears very likely that the lateral displacements (kinks) of the jet axis are systematic and reflect a general jet property in 0836+710.

At smaller separations from the core, two new components B2 & B3 are seen (Figure 3). Linear back-extrapolation of the motion of B2 allows its identification with a component previously visible in a 5 GHz map of 1990 (O96). Adopting its constant apparent speed of $\beta_{app} = 8.3 \pm 2$, the component B2 was ejected before 1986.8 and therefore cannot be related to the flare observed in 1992.

In the 22 GHz map of 1993.71, the core appears elongated, indicating the emergence of a new component (see Fig. 3, left). From Gaussian model fits we determined its relative separation from the core of $r \simeq 0.3$ mas. We label this component B3. The image of 1995 (Fig. 3, right) shows B3 at $r \simeq 0.8$ mas,

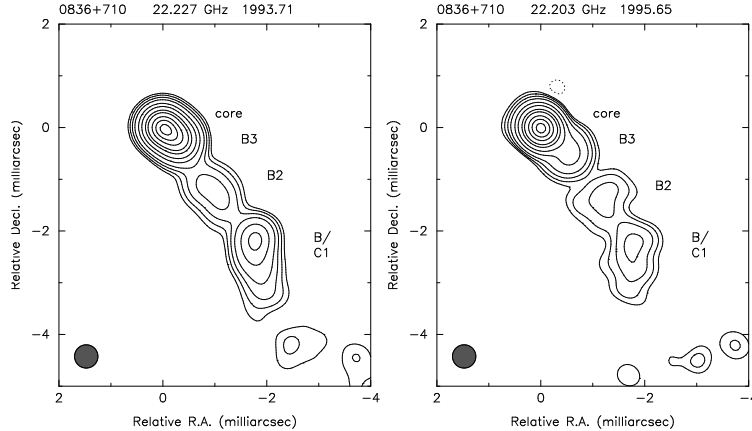


Fig. 3. 22 GHz maps of the inner jet of 0836+710 from 1993.71 (left) and 1995.65 (right). Contour levels are $-0.25, 0.25, 0.5, 1, 2, 5, 10, 20, 30, 50, 70, 90\%$ of the peak flux density of 0.35 Jy/beam (left), and 0.9 Jy/beam (right). Both maps are restored with a circular beam of 0.45 mas size. Labels denote the component identification.

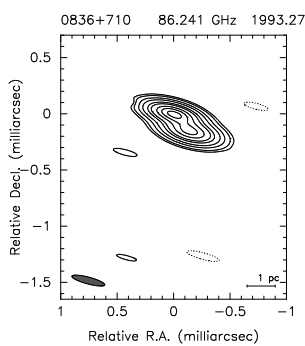


Fig. 4. 86 GHz map of 0836+710 of 1993.27. Contour levels are $-1, 1, 2, 5, 10, 20, 30, 50, 70, 90\%$ of the peak flux density of 0.41 Jy/beam. The observing beam size is 0.30×0.06 mas, P.A. = 75° .

thus indicating superluminal motion with a speed similar to its predecessors B2 and B (see next paragraph).

The ejection of a new component and its subsequent separation from the core is further supported by mm-VLBI observation of the source. A high angular resolution map obtained at 86 GHz in 1993.27 (Fig. 4), 5 months earlier than our first 22 GHz observation, showed a secondary component next to the unresolved VLBI core (size ≤ 0.1 mas). Owing to the small number of participating VLBI stations at this high observing frequency and the resulting limitations of the uv -coverage, the 86 GHz map shows only the most prominent features of a probably more complex brightness distribution. The secondary component is located at $r \simeq 0.15$ mas. Since its po-

Table 2. Relative separation from the core of the new component B3

epoch	freq. [GHz]	R [mas]	PA [$^\circ$]
1993.27	86	0.15 ± 0.05	220 ± 20
1993.71	22	0.34 ± 0.04	231 ± 3
1995.05	15	0.72 ± 0.15	227 ± 5
1995.65	8	0.69 ± 0.15	229 ± 5
1995.65	22	0.76 ± 0.06	230 ± 3
1996.34 ¹	22	1.05 ± 0.10	–

Notes: ¹: A. Marscher, priv. comm.

sition agrees well with the extrapolated position of B3 (from 22 GHz data) at that time, we identify this component with B3.

3.2.2. Motion of component B3

In Table 2, we summarize the relative separations of B3 from the core for all available observing epochs. We further added a data point from a 22 GHz map of 1996.34, which was kindly provided by A. Marscher (priv. comm.).

In synchrotron self-absorbed VLBI jets (e.g. Blandford and Königl 1979), frequency dependent shifts of the relative positions of the VLBI components, caused by optical depth effects, are expected. The comparison of the relative component positions between the nearly simultaneous 8, 15 and 22 GHz images, however, indicate that the position shifts in 0836+710 are relatively small ($\lesssim 0.1$ mas). In the following, we neglect such shifts due to opacity and plot in Figure 5 the relative separation from the core of B3 versus time. The data points line up very

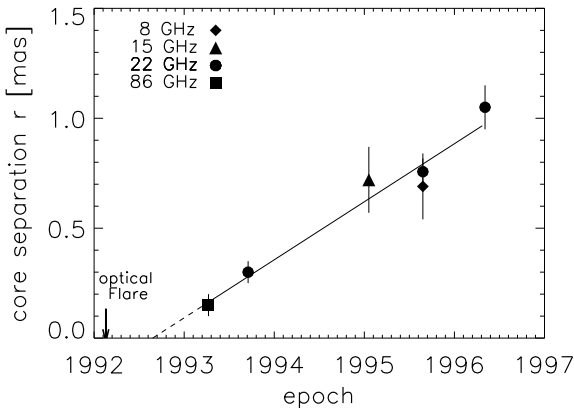


Fig. 5. Relative separation of component B3 from the core plotted versus time. Symbols denote different frequencies: diamonds (8 GHz), triangles (15 GHz), circles (22 GHz), and squares (86 GHz). The solid line represents a linear fit with slope $\mu = 0.26$ mas/yr, corresponding to superluminal motion with $\beta_{\text{app}} = 10.8$. Linear back-extrapolation (dashed line) yields component ejection near 1992.65. The arrow indicates the onset of the optical flare (1992.13).

nicely, thus confirming indirectly the validity of our assumption of negligible opacity effects. Furthermore, we find no evidence for non-linear motion, e.g. acceleration or motion along curved paths (see also the nearly constant position angle of B3 in table 2).

A linear fit to the data yields an apparent angular separation rate of $\mu = 0.26 \pm 0.03$ mas/yr corresponding to an apparent velocity of $\beta_{\text{app}} = 10.8 \pm 1.3$. This velocity is close to the speeds seen for the older components B & B2 (K90b, O96), and confirms the previous finding of relatively high velocities at small separations from the core (note: components C1 and C2 move substantially slower, cf. K90b). Linear back-extrapolation of the motion of B3 yields the time of zero separation of $t_{\text{ej}} = 1992.65^{+0.15}_{-0.17}$. This is close to the time of the strong optical flare observed in 1992.13 (von Linde et al. 1993, see Figure 2). Within possible extrapolation errors and due to the limited and partially incomplete time coverage of the optical flaring, it therefore appears that B3 was ejected *during or shortly after* ($0 \lesssim \Delta t \leq 0.67$ yrs) the optical outburst. We study the correlation between the optical flaring and the ejection time of B3 in more detail in section 4.2.

3.3. Evolution of the total radio spectrum

Figure 2 shows the propagation of the outburst through the spectrum. Such a behavior is readily described within the standard shock-in-jet models (e.g. Marscher & Gear 1985), in which a relativistic shock propagates along a synchrotron self-absorbed jet, causing (at least qualitatively) the observed frequency dependence.

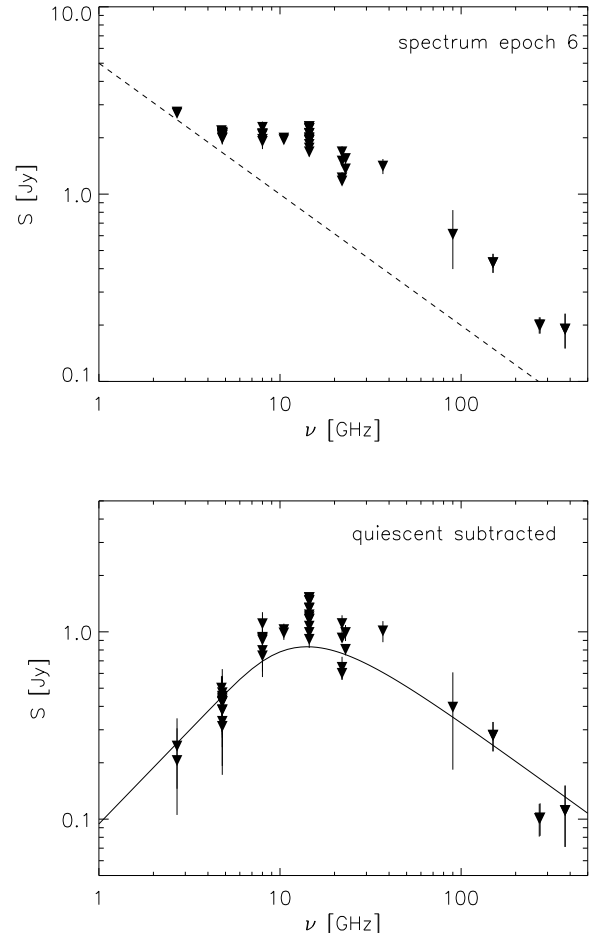


Fig. 6. Spectrum of 0836+710 at epoch 6 (1992.75). In the upper picture the total spectrum is plotted. The dashed line shows the quiescent spectrum, i.e. the quiescent part determined from an observations prior to the optical flare in 1992. In the lower panel the residual variable part of the spectrum (quiescent spectrum subtracted) and the fit used to determine the spectral turn over is shown.

From the data shown in Figure 2 and additional data from measurements made with the MPIfR 100 m radio telescope at longer cm-wavelengths, we are able to follow the evolution of the radio spectrum and to determine the path of a local spectral excess, which propagated from higher to lower frequencies.

From our radio data, we first constructed quasi-simultaneous radio spectra covering the 1.4 – 230 GHz range. Good spectral coverage is achieved in the period from 1992.05 to 1993.00. To overcome the lack of frequency coverage at individual epochs, we binned the available data into 7 intervals, each of 50 days in duration. Since the source did not show strong variations within the binning-timescale, we are confident that the averaging of the data within each bin is not causing large errors for our later derived turnover points. Figure 6 (top) gives an example of such a radio spectrum.

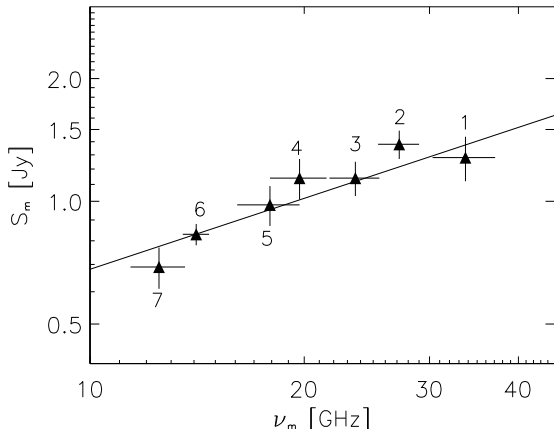


Fig. 7. Path of the spectral evolution of the turnover point in the $S_m - \nu_m$ -diagram. The labels 1–7 denote the individual spectral epochs (see text). The straight line shows a power law fit ($S_m \propto \nu_m^{0.58}$) to the data.

The long-term flux density monitoring of 0836+710 at cm-wavelengths shows longer periods of low or only moderately slow (timescales of \sim years) variability. One such period had occurred prior to the time of the optical activity in 1992. We used the spectra from this period to determine the shape of the quiescent spectrum (non-variable part). Throughout the radio band considered (~ 1 –100 GHz) it can be well represented by a simple power law ($S_\nu \propto \nu^{-0.7}$), which we plot as dashed line in Figure 6 (top).

In order to determine the position (ν_m, S_m) of the turnover point of the variable part of the radio spectrum, we now subtracted the same quiescent spectrum from our binned spectra. The fit of a homogeneous synchrotron component spectrum (with spectral indices $\alpha_{\text{thick}} = 2.5$ and $\alpha_{\text{thin}} = -0.7$) to each of the residual spectra was rather unsatisfactory, indicating that the variable part of the radio spectrum cannot be represented well enough by a single and homogeneous synchrotron component. A much better fit was achieved when we used $\alpha_{\text{thick}} = 1.0$ and $\alpha_{\text{thin}} = -0.7$. In the following we use the results from these fits. Figure 6 (bottom) shows an example of such a fit for one of the spectra (epoch 6). From each of the fits to the 7 residual spectra, we determined the position of the spectral turnover. In Figure 7 the turnover flux density S_m is plotted versus turnover frequency ν_m as a function of time. The numbered labels at each position correspond to the following epochs: 1 - 1992.07 (TJD 8650), 2 - 1992.21 (TJD 8700), 3 - 1992.35 (TJD 8750), 4 - 1992.48 (TJD 8800), 5 - 1992.62 (TJD 8850), 6 - 1992.76 (TJD 8900), 7 - 1992.90 (TJD 8950).

The measured path of the spectral turnover seems to follow a linear trend (in the $\log(S_m)/\log(\nu_m)$ space), which can be interpreted within models invoking a shock moving along a relativistic synchrotron self-absorbed jet. In the model of Marscher & Gear (1985) and Marscher (1990), the spectral evolution is described by three subsequent phases of energy loss and radi-

ation, the Compton, synchrotron, and adiabatic phase. During the first two stages, the turnover flux rises with decreasing frequency, then remains nearly constant. The phase of adiabatic losses is characterized by a decrease of the flux density with decreasing turnover frequency. We therefore identify the spectral evolution seen in Figure 7 with the adiabatic–loss stage. A power law fit (the straight line in Figure 7) to the path of the turnover point yields $S_m \propto \nu_m^{0.58}$.

We note that in Figure 7 a slightly steeper slope is obtained, if the first data point (point no. 1) is not included in the fit. Within the afore mentioned model, it is possible that the spectral evolution from point no. 1 to no. 2 reflects the transition from the synchrotron to the adiabatic cooling phase. If this is the case, the synchrotron loss dominated phase would have ceased $t_{\text{sync}} < 30$ days after the onset of the optical flare. Obviously observations much closer to the time of the outburst would have been required to study the synchrotron phase.

4. Discussion

4.1. The total spectrum and the VLBI jet

The $S_m - \nu_m$ dependence determined in the previous section can be used for studying the relation between the spectral and kinematic properties of the relativistic jet in 0836+710. Despite some evidence for emission from an inhomogeneous synchrotron component ($\alpha_{\text{thick}} = 1.0$, see previous section), we postulate for the sake of simplicity, that the observed spectral variations are produced by a single, compact relativistic shock dominating the source radio emission, and associated with the core of the jet or an emitting region moving inside the jet within $\lesssim 0.1$ mas distance from the core (a distance comparable to the back-extrapolated separation of B3 at the last spectral epoch, 1992.9). We use the formalism developed by Marscher & Gear (1985), and account for possible variations of the Doppler factor in the emitting region (Marscher 1990). Based on the synchrotron spectral index $\alpha = -0.7$ used for the spectral fitting, a power law electron energy distribution with $s = 2.4$ ($s = 1 - 2\alpha$) is assumed. The magnetic field distribution along the jet axis r is defined by an exponent a , so that $B \propto r^{-a}$. The Doppler factor is $\delta \propto r^b$. The spectral evolution of the shock is then described by the variations of the turnover point: $S_m \propto \nu_m^\rho$ and $\nu_m \propto r^\epsilon$. The exponents ρ and ϵ depend on the dominating type of the energy losses (Marscher 1990, Marscher et al. 1991, Lobanov & Zensus 1998). Following Marscher (1990), we obtain the following expressions for ρ and ϵ during the adiabatic–loss stage:

$$\rho = -\frac{(19 - 4s) - 3a(2s + 3) + 3b(3s + 7)}{2(2s + 1) + 3(a - b)(s + 2)}, \quad (1)$$

$$\epsilon = -\frac{2(2s + 1) + 3(a - b)(s + 2)}{3(s + 4)}. \quad (2)$$

We now consider two cases: a) a jet with transversal ($a = 1$) magnetic field, and b) a jet with longitudinal ($a = 2$) magnetic field. With the measured $\rho = 0.58$, changes of the Doppler

factor and turnover frequency along the jet can be determined from (1) and (2).

For $a = 1$, we obtain $b = 0.0$ and $\epsilon = -1.3$. The distance travelled by the emitting region between 1992.07 and 1992.90 (the 1st and the 7th spectral epochs) should increase by a factor of $r_7/r_1 \approx 2.1$. To assess the jet kinematics, we use $\beta_{\text{app}} = 10.8$ measured in Section 3.2.2 for the jet component B3 at small separations from the core. For now, we assume that the jet bulk Lorentz factor is $\gamma_j = 10.9$, with the resulting Doppler factor $\delta_j = 11.4$ and jet viewing angle $\theta_j = 5^\circ$. Using the time separation between the two aforementioned spectral epochs, $\Delta t = 0.83$ yrs, one can then estimate the distance between the emitting region and the jet apex, $r_1 = \beta\gamma\delta\Delta t/(1+z) = 9.5 \pm 0.8$ pc.

The case with $a = 2$ results in $b = 0.4$, implying that the emitting region was accelerating. The corresponding turnover frequency evolution is described by $\epsilon = -1.7$. The resulting Doppler factor must increase between t_1 and t_7 by $\delta_7/\delta_1 = (\nu_{\text{m}7}/\nu_{\text{m}1})^{b/\epsilon} \approx 1.3$, and the corresponding distance must become larger by a factor of ≈ 1.8 . For a jet with variable Doppler factor, the distance travelled by the shock between two epochs t_1 and t_2 is (Lobanov & Zensus 1998):

$$\Delta r_{1,2} = (1+z)^{-1} \int_{t_1}^{t_2} \frac{\beta(t) dt}{1 - \beta(t) \cos \theta(t)}. \quad (3)$$

For the Doppler factor $\delta \propto r^b$, equation (3) gives for the distance to the jet apex at the epoch t_1 :

$$r_1 = \left(\frac{1+z}{\delta_1 c \Delta t} \int_1^{r_u} \frac{1}{\sqrt{\gamma^2(r) - 1}} \frac{dr}{r^b} \right)^{1/(b-1)}, \quad (4)$$

where c is the light speed, $\Delta t = t_2 - t_1$, and $r_u = (\nu_{\text{m}2}/\nu_{\text{m}1})^{1/\epsilon}$. The exact form of $\gamma(r)$ is essentially unknown. In many cases, it can be assumed to be constant (so that the Doppler factor variations are entirely due to a curved path followed by the emitting region). For a straight jet, the $\gamma(r)$ can be derived from the Doppler factor variations. For 0836+710, both approaches yield similar result: $r_1 \sim 30$ pc (here we postulate $\delta_7 = \delta_j$). One can argue that the location r_1 (the beginning of the adiabatic-loss stage) should correspond to the VLBI core, since the core emission is likely to be dominated by Compton and synchrotron energy losses (Unwin et al. 1994, 1997), whereas the moving jet components are successfully modelled as adiabatically expanding spherical plasmons embedded in the jet (Zensus et al. 1995). In view of this argument, the case of a non-accelerating jet with $r_1 \approx 10$ pc appears to be more likely to explain the observed spectral behavior in 0836+710.

4.2. Travel times and radio-to-gamma correlations

If the jet core is located at r_1 , one can calculate the travel time between the jet nozzle, r_0 , and the core. For $b = 0$ ($\delta = \text{const}$), the calculation is trivial, and it gives (in the observer's frame) $\Delta t_{0,1} = (1+z)r_1\gamma^{-1}\delta^{-1}\beta^{-1} = 0.74 \pm 0.07$ yrs. For an accelerating jet, the travel time can be calculated from (3), and it depends on the (unknown) Doppler factor δ_0 at the jet nozzle. If the nozzle is formed by a pressure drop in a relativistic

outflow, the resulting Lorentz factor is $\gamma_0 \approx 1.2$ (Marscher 1980). The corresponding Doppler factor is then $\delta_0 \approx 1.8$, for $\theta_0 = \theta_j = 5^\circ$. The resulting travel time is $\Delta t_{0,1} = 1.6$ yrs. For larger γ_0 , the travel time increases and may become as large as 2.8 yrs, if $\gamma_0 \approx \gamma_1$.

On the basis of the arguments presented in the previous section, we take $\Delta t_{0,1} = 0.74$ yrs as a better estimate of the travel time between the nozzle and the core. In section 3.2.2, we have found $t_{\text{ej}} = 1992.65$ for the ejection time of the superluminal feature B3. Together with the derived nozzle-to-core travel time, this implies that the plasma condensation responsible for the emission of B3 had travelled through the nozzle at $t_0 = 1991.91 \pm 0.21$. The latter epoch is very close to the time when the optical flare was observed in the source. Although the coincidence may be only fortuitous, it is rather striking, and we would like to emphasize that such a situation is indeed possible. For instance, if a flare occurs when a dense plasma condensation travels through the jet sonic point, the optical depth in the radio bands can exceed unity, and only a high-energy flare (optical, X-rays, or gamma-rays) is observed. An increase of the radio emission and the associated ejection of a new VLBI feature are observed later, after the condensation has travelled outside the $\tau \geq 1$ region.

The jet geometry and travel times above are determined for $\gamma_j \approx \gamma_{\text{min}}$. If we suppose that the gamma-to-optical flaring activity and the ejection of VLBI component B3 in 1992 had a common origin, the jet geometry can be uniquely determined. We assume that the maximum of the flare occurs at $t_{\text{flare}} = 1992.13$ and take $t_{\text{ej}} = 1992.65$ from the extrapolation of the component motion. In such a scenario, $\Delta t_{0,1} = t_{\text{ej}} - t_{\text{flare}}$, and we find $\gamma_j = 11.8$ and $\theta_j = 3.2^\circ$. The corresponding Doppler factor is $\delta_j = 16.4$; the core-to-nozzle distance is $r_1 \approx 15$ pc. We note that the derived values are consistent with overall kinematics of 0836+710 (O96). We therefore view this model as a likely explanation for the kinematic properties, spectral behavior and flaring activity observed in 0836+710 in 1992–1993.

4.3. Properties of the inner jet

The kinematic parameters determined above for the case of a non-accelerating ($b = 0$) jet with transverse ($a = 1$) magnetic field can be further used to evaluate the physical conditions in the emitting region responsible for the observed spectral changes in 0836+710. For this purpose, we associate the core-to-nozzle distance, $r_1 = 15$ pc with the location of the emitting region at the estimated epoch of origin of B3 ($t_{\text{ej}} = 1992.65$). Then, for each spectral epoch, we find the respective location,

$$r = r_1 \left(\frac{\nu_m}{\nu_1} \right)^{1/\epsilon}, \quad (5)$$

and size of the emitting region (using equation (3) from Marscher 1987),

$$d = d_1 \left(\frac{\nu_1}{\nu_m} \right)^{(5\epsilon+a+b)/4\epsilon} \left(\frac{S_m}{S_1} \right)^{1/2}. \quad (6)$$

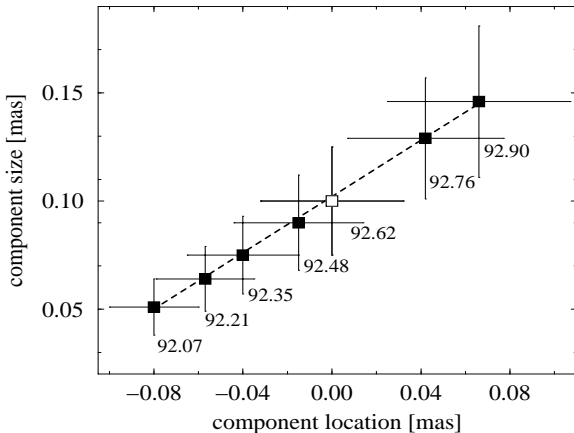


Fig. 8. Projected location and size of the emitting feature as derived from the observed spectral evolution. The locations of the emitting feature are calculated assuming a viewing angle of $\theta_j = 3^\circ 2$ obtained from equating the core-to-nozzle travel time with the observed time-lag between the gamma-flare and the ejection of B3. The respective spectral epochs 1–7 are given next to the data points. Open square denotes the location of the VLBI-core of 0836+710. The increase of the size of the emitting region can be modeled by a conical jet with an opening angle $\phi_j = 2^\circ 1 \pm 0^\circ 1$.

S_1 and ν_1 are measured at t_{ej} , which gives $\nu_1 = 17.9 \pm 1.8$ GHz and $S_1 = 0.98 \pm 0.11$ Jy. For d_1 , we use the size of the VLBI core, $\Omega_{\text{core}} \approx 0.1$ mas, typically measured in the 22 GHz images of 0836+710. The corresponding linear size is $d_1 = 0.4$ pc.

The derived projected location and size of the emitting region are shown in Figure 8 for all spectral epochs. The open square refers, in Figure 8, to the back-extrapolated ejection epoch of B3 (associated with the passage of B3 through the VLBI core). At earlier epochs, the emitting region was optically thick at frequencies $\nu \leq 22$ GHz, which is reflected in its negative location with respect to the VLBI core (implying that the emitting region was traveling between the jet base and the VLBI core). The region was expanding almost linearly; the resulting opening angle $\phi_j = 2^\circ 1 \pm 0^\circ 1$ is in a good agreement with the observed opening angle measured in the immediate vicinity of the VLBI core (O96). During the expansion, the magnetic field decreases from ≈ 0.2 G to ≈ 0.05 G, with the core magnetic field, $B_{t=1992.62} \approx 0.1$ G.

With the jet parameters determined, we can now discuss the energy balance in the compact jet of 0836+710. We adopt the formulation of Blandford and Königl (1979) to estimate the total (kinetic+magnetic field) power of the jet, $L_{\text{tot}} = 2.0 \cdot 10^{48}$ erg s $^{-1}$. The corresponding synchrotron power of the jet is $L_{\text{syn}} = 2.5 \cdot 10^{47}$ erg s $^{-1}$. The data from von Linde et al. (1993) provide an estimate of the energy deposited in the jet by the optical flare, $E_{\text{opt}} \approx 2 \cdot 10^{47}$ erg. The maximum observed gamma luminosity of 0836+710 is $\approx 1.8 \cdot 10^{48}$ erg s $^{-1}$ (Mukherjee et al. 1997), but it should be made smaller by 10^2 – 10^3 to account

for Doppler boosting of the gamma-radiation. Comparing the optical energy output and gamma luminosity to the jet radio power, we can conclude that flaring activity is not likely to play a significant role in forming and maintaining the jet. On the other hand, we find that the average isotropic luminosity of the optical flare is similar to the isotropic radio luminosity observed at the epoch of the flare ($\approx 4 \cdot 10^{45}$ erg s $^{-1}$), suggesting the relation between the emission in the two bands. In our view, this supports the schemes in which relativistic electrons (responsible for synchrotron emission in the radio and optical bands) are the primary radiating particles in the jet, and external photons (producing the observed gamma-emission) are Compton scattered by the jet electrons (e.g. Blandford & Levinson 1995). Then the energy densities of the synchrotron and Compton emission can be related through the Doppler factor, so that $u_C/u_{\text{syn}} = k_e \delta_{\text{eq}}^{1-\alpha_C}$, (Dermer, Sturner & Schlickeiser 1997). We assume equipartition ($k_e = 1$) between the external radiation field and the magnetic field of the emitting region. Then, for a typical spectral index of Compton emission, $\alpha_C = -1.0$, we obtain $\delta_{\text{eq}} = 15.3_{-1.1}^{+1.5}$, which is consistent with the $\delta_j = 16.4$ derived in section 4.2.

5. Summary

High frequency VLBI-observations performed shortly after a strong gamma/optical/radio outburst in the quasar 0836+710 revealed the ejection of a new jet component, which is moving at a constant apparent speed of $\beta \sim 10$. Back-extrapolation of the motion yields a time of ejection of the component shortly (< 0.7 yrs) after the time of the gamma/optical flaring. The monitoring of the variations in total radio spectrum showed a synchrotron self-absorbed spectral component propagating from high to low frequencies. The path of the spectral turnover of this component, which we identify with the ejected jet component, is consistent with adiabatic expansion at a slope of $S_m \propto \nu_m^{0.6}$. The time lag between the outburst and the observed component ejection can be quantitatively explained by strong synchrotron self-absorption at the jet base, which prevents the detection of the radio emission from the component at early epochs. In this model, the jet radio-core is separated by ≈ 15 pc from the jet base. The jet plasma has a bulk Lorentz factor $\gamma_j \approx 12$, and moves at an angle of about 3° to the line of sight. The corresponding jet opening angle derived from the expansion of the spectral component is $\phi_j = 2^\circ 1$. The derived values are consistent with the jet kinematic parameters obtained from VLBI monitoring of the source (O96).

The high gamma-ray luminosity (Figure 1) of 0836+710, which surpasses the IR/optical luminosity by at least one order of magnitude, the rapid and apparently correlated variability seen in the gamma-ray and the optical regimes (Figure 2), and the ejection of a highly superluminal ($\beta_{\text{app}} = 10$) jet component after the quasi-simultaneous optical/gamma-ray flaring, strongly supports the idea that the gamma-emission originates in the inner parts of a highly relativistic jet and that a broadband correlation – perhaps extending over the full electromag-

netic spectrum – between high energy outbursts and ejection of new jet components exists.

The observed multi band energy output during and after the flare in 1992.1 allows us to conclude that the gamma and optical flaring activity are not sufficient to maintain the jet total power, but are connected with the observed jet radio emission. In this scheme, relativistic electrons are responsible for synchrotron emission in the optical and radio bands, and external Compton scattered photons produce the observed gamma radiation.

Acknowledgements: We thank A. Marscher and A. Patnaik for providing data prior to publication and H. Teräsranta and E. Valtaoja for their flux density measurements at 22 & 37 GHz. We also thank H. Bock for analysis of parts of the optical data and J. von Linde for help calibrating the optical data. We thank I. Pauliny-Toth for careful reading of the manuscript. The work of T. P. K. was supported in part from a grant of the German Verbundforschung of the BMBF. S. J. W. was supported by a grant of the DFG (SFB 328).

The VLBA is a facility of the NRAO, which is operated by Associated Universities Inc., under cooperative agreement with the NSF.

This research has made use of data from the University of Michigan Radio Astronomy Observatory which is supported by the National Science Foundation and by funds from the University of Michigan.

References

Alef W., Porcas R. W., 1986, A&A 168, 365.

Alef W., 1989, in: *Very Long Baseline Interferometry; Techniques and Applications*, eds. M. Felli and R.E. Spencer (Kluwer: Dordrecht), p. 97.

Babadzhanyants M. K., Belokon E. T., 1986, Astrophysics 23, 639.

Blandford R.D., Königl A., 1979, ApJ 232, 34.

Blandford R. D., Levinson A., 1995, ApJ 441, 79.

Bloom S.D., Marscher A.P., Gear W.K., et al. 1994, AJ 108, 398.

Brunner H., Lamer G., Staubert R., Worall D. M., 1994, A&A 287, 436.

Cawthorne T. V., Wardle J. F. C., Roberts D. H., Gabuzda D. C., Brown L. F., 1993, ApJ 416, 496.

Dermer C.S., Sturner, S.J., Schlickeiser R., 1997, ApJS 109, 103.

Eckart A., Witzel A., Biermann P. et al., 1986, A&A 168, 17.

Eckart A., Witzel A., Biermann P. et al., 1987, A&AS 67, 121.

Fichtel C. E. Bertsch D. L., Chiang J. et al., 1994, ApJS 94, 551

Hummel C. A., Muxlow T. W. B., Krichbaum T. P. et al., 1992, A&A 266, 93.

Krichbaum T. P., Booth R. S., Kus A. J. et al., 1990a, A&A 237, 3.

Krichbaum T. P., Hummel C. A., Quirrenbach A. et al., 1990b [K90b], A&A 230, 271.

Krichbaum T.P., Britzen S., Standke K. J. et al., 1995, in: *Quasars and Active Galactic Nuclei: High-Resolution Radio Imaging*, ed. M.H. Cohen and K.I. Kellermann, Proc. Nat. Acad. Sci. USA, Vol. 92, No. 5, p. 11377.

Krichbaum T.P., Otterbein K., Britzen S. et al., 1996, in: Proceedings of the Heidelberg Workshop on Gamma-Ray Emitting AGN, ed. J.G. Kirk, M. Camenzind, C. von Montigny, & S. Wagner, (MPI-preprint MPI H - V37 - 1996: Heidelberg), p. 96.

<http://www.lsw.uni-heidelberg.de/projects/extragalactic>

Kühr H., Pauliny-Toth I. I. K., Witzel A., Schmidt J., 1981, AJ 86, 854.

von Linde J., Borgeest U., Schramm K.-J. et al., 1993, A&A 267, L23.

Lobanov A. P., Zensus J. A., 1998, ApJ (submitted)

Marscher A. P., 1980, ApJ 235, 386.

Marscher A. P., Gear W. K., 1985, ApJ 298, 114.

Marscher A. P., 1987, in: *Superluminal radio sources*, ed. Zensus J. A., Pearson T. J., Cambridge University Press, p. 280.

Marscher A. P., 1990, in: *Parsec-Scale Radio Jets*, ed. Zensus J. A., Pearson T. J. (NRAO, Socorro), p. 236.

Marscher A. P. and Bloom S. D., 1994, in: *Compact Extragalactic Radio Sources*, ed. J.A. Zensus and K.I. Kellermann (NRAO, Socorro), p. 179.

Marscher A. P., Gear W. K., Travis J. P., 1992, in: *Variability of Blazars*, ed. E. Valtaoja and M. Valtonen, Cambridge University Press, p. 85.

Mukherjee R., Bertsch D. L., Bloom S. D., et al., 1997, ApJ 490, 116.

Mutel R. L., Phillips R. B., Bumei Su, Bucciferro R. R., 1990, ApJ 352, 81.

Otterbein K., 1996 [O96], PhD thesis, University of Göttingen.

Patnaik A., Garrett M.A., Polatidis A., & Bargi D., 1996, in: *Astrophysical Applications of Gravitational Lensing*, IAU Symp. No. 173, eds. C.S. Kochanek and J.N. Hewitt (Kluwer: Dordrecht), p. 405.

Pearson T. J., 1991, BAAS 23, 991.

Shepherd M.C., Pearson, T.J., Taylor G.B., 1994, BAAS 26, 987.

Rogers, A.E.E., Capallo R.J., Hinteregger H.F., et al. 1983, Sci 219, 51.

Schalinski C.J., Witzel A., Krichbaum T.P., et al., 1994, in: *Compact Extragalactic Radio Sources*, ed. J.A. Zensus and K.I. Kellermann (NRAO, Socorro), p. 45.

Schramm K.-J., Borgeest U., Kühl D., von Linde J., Linnert M. D., Schramm T., 1994, A&AS 106, 349.

Steppe H., Paubert G., Sievers A. et al., 1993, A&AS 102, 611.

Unwin S.C., Wehrle A.E., Urry C.M. et al. 1994, ApJ 432, 103.

Unwin S.C., Wehrle A.E., Lobanov A.P. et al. 1997, ApJ 480, 596.

Wagner S. J., Camenzind M., Dreissigacker O. et al., 1995a, A&A 298, 688.

Wagner S. J., Mattox, J.R., Hopp U. et al., 1995b, ApJL 454, 97.

Wehrle A.E., Zock A.C., Unwin S.C., 1994, *The Multimission Perspective* (Eureka Scientific: Napa Valley CA), p. 27.

Witzel A., Schalinski C.J., Johnston K. J. et al., 1988, A&A 206, 245.

Zensus J. A., Cohen M. H., Unwin S., 1995, ApJ 443, 35.